EEET ECOLOGICAL ENGINEERING & ENVIRONMENTAL TECHNOLOGY

Ecological Engineering & Environmental Technology, 2026, 27(8), 376–390
https://doi.org/10.12912/27197050/225416
ISSN 2719–7050, License CC-BY 4.0

Received: 2026.06.18
Accepted: 2026.07.10
Published: 2026.08.01

Spatial variability of soil properties in hydromorphic mangrove soils in Diawling National Park (Mauritania)

Sidi Mohamed Cheikh Ouedi[1,2*], Mohamed Mahmoud Abidine[1], Hela Ben Ahmed[2], Alessandro Crisafulli[3], Rosa Maria Picone[3], Ahmedou Vadel Salihi[1,4]

[1] Biodiversity and Valorization of Biological Resources Unit, Faculty of Science and Technology, University of Nouakchott, Nouakchott, Mauritania
[2] Plant-Soil-Environment Interaction Laboratory, Faculty of Sciences Tunis, El Manar University, Tunisia
[3] Department of ChiBioFarAm, University of Messina, 98166 Messina, Italy
[4] Higher Institute of Biotechnology, University of Nouadhibou, Nouadhibou, Mauritania
* Corresponding author's e-mail: sidicheikhweddy@gmail.com

ABSTRACT

The mangroves of Diawling National Park (PND) in Mauritania form an ecosystem of high ecological value that is exposed to severe climatic and anthropogenic pressures. This study analyses the spatial variability of four soil physicochemical properties (electrical conductivity (EC), pH, soil organic carbon (SOC) and total nitrogen (N)) and compares two spatial interpolation methods, inverse distance weighting (IDW) and ordinary kriging (OK). Fifty samples were taken at a depth of 20 cm beneath stands of Avicennia germinans and Rhizophora racemosa and analysed in the laboratory. The descriptive statistics show pronounced variability for EC (CV = 38.4%) and SOC (CV = 35.9%), whereas pH (CV = 10.2%) and N (CV = 16.4%) are distributed more evenly. The mean organic carbon content (0.680%) falls below the values reported for humid tropical mangroves, a difference that reflects the combined saline and water stress affecting Sahelian mangroves. Cross-validation based on six statistical criteria (ME, RMSE, R, MSE, RMSSE, ASE) confirms the clear advantage of IDW, whose correlation coefficients approach unity (R > 0.999) for all four properties, while OK performs more unevenly, from very weak for pH (R = 0.091) to moderate for EC and SOC (R = 0.647 and 0.445) and good for N (R = 0.989). Semivariogram modelling shows a nugget-to-sill ratio of 0.7569 for EC, denoting weak spatial dependence, and a fitted nugget exceeding the fitted sill for pH, SOC and N (ratios of 5.3158, 2.9924 and 16.3692, respectively), a pattern functionally equivalent to a pure nugget effect; together these results reveal that unstructured short-range variability dominates the spatial signal of all four properties and provide a mechanistic basis for the systematic underperformance of OK. This contrast stems from the strong short-range heterogeneity produced by the redox processes typical of the hydromorphic environment, which weakens geostatistical approaches that depend on structured spatial autocorrelation. The IDW maps display an organised spatial pattern, with a salinity gradient that follows hydraulic connectivity and a mosaic of pH values governed by local redox cycles. These results offer a spatial reference for managing and conserving the PND mangroves and add to the understanding of biogeochemical processes in mangrove ecosystems at the Sahelian margin.

Keywords: Mangrove, soil physicochemical properties, spatial variability, inverse distance weighting, ordinary kriging, Diawling National Park, Mauritania.

INTRODUCTION

Mangroves are coastal wetlands that occur along tropical and subtropical shorelines. They deliver a broad set of ecosystem services that includes nutrient cycling, soil formation, timber production, pollution control, ecotourism, aquaculture and carbon sequestration (Feng et al., 2019; Gao et al., 2019; Murdiyarso et al., 2015; Wang et al., 2024; Yin et al., 2023). Their high capacity to store carbon comes from elevated primary productivity combined with anoxic soils that slow decomposition (Murdiyarso et al., 2015; Xia et al., 2022). Because they can lower atmospheric CO_2 over long periods, conserving mangroves is widely regarded as an effective response to climate change (Suello et al., 2022; Xu et al., 2024). Over the past few decades these ecosystems have been heavily degraded by human pressures (Feng et al., 2019; Yan et al., 2024), and restoration programmes now seek to rebuild lost habitats and recover degraded functions (Feng et al., 2019; Maietta et al., 2020). Soil organic carbon (SOC) ranks as the third-largest carbon reservoir on Earth, behind the oceanic and geological pools (Lal et al., 1999; Shi et al., 2017). It is especially important in mangroves, where the soil holds the greater part of the total ecosystem carbon stock (Bernal and Mitsch, 2012; Luo et al., 2017; Yin et al., 2023). Such differences probably arise from the combined influence of climate, soil physicochemical properties and land management on carbonate precipitation and dissolution (Shi et al., 2017). The controls on mangrove SOC nevertheless remain complex, since they depend on several interacting physicochemical factors, among which pH, electrical conductivity (EC) and total soil nitrogen rank among the most important (Hu et al., 2024; Xia et al., 2021). Total nitrogen (TN) has emerged as a key driver of carbon storage in mangroves, particularly in nitrogen-poor systems where its availability governs both primary production and the stabilization of organic matter (Hu et al., 2024; Xia et al., 2021). Restored mangroves show very strong TN-SOC correlations ($r > 0.95$), which indicates that bioavailable nitrogen accumulates alongside carbon as ecological succession proceeds (Ray et al., 2023; Wang et al., 2023). Soil pH also shapes SOC dynamics, both spatially and functionally, through its effect on organic-matter decomposition, nutrient availability and the structure of microbial communities along land-sea gradients (Dookie et al., 2024; Zheng et al., 2025). Electrical conductivity, closely tied to salinity and dissolved-ion concentration, is a third control on SOC; it acts on mineralization, on the input of allochthonous organic matter and on particle-organic matter interactions (Cui et al., 2021; Ray et al., 2023). Negative EC-SOC correlations have been recorded along restored transects ($r = -0.24$), which suggests that more saline or high-EC settings may depress measured SOC (Ray et al., 2023). Large-scale syntheses likewise rank salinity, or EC, among the main determinants of how SOC stocks are distributed across mangroves (Chowdhury et al., 2023; Wu et al., 2025). In the lower Senegal River delta, and specifically within Diawling National Park (PND), soil salinisation has been identified as a major source of environmental imbalance (Abidine et al., 2018; Ngom et al., 2016; Nuscia Taïbi et al., 2007). It drives the decline of sensitive plant communities and favours halotolerant species better suited to saline conditions (Abidine et al., 2018). Understanding the link between soil salinity and plant behaviour is therefore essential for assessing the functioning and resilience of these mangroves (Herbert et al., 2018). Because soil physicochemical properties vary markedly in space, mapping environmental gradients in mangroves calls for suitable geostatistical and spatial interpolation techniques (Robinson and Metternicht, 2006; Tripathi et al., 2015). These methods estimate soil parameters at unsampled locations from point measurements and produce the continuous maps needed to study processes such as salinization (Bhunia et al., 2018; Emadi and Baghernejad, 2014). The techniques in common use range from deterministic approaches, such as inverse distance weighting (IDW), to probabilistic geostatistical ones, such as ordinary kriging (OK) (Robinson and Metternicht, 2006; Zarco-Perelló and Simões, 2017). Both have frequently been applied to map pH, electrical conductivity and other properties such as total nitrogen. Comparing them through statistical performance criteria is necessary in order to choose the technique best suited to a given parameter and soil context (Bhunia et al., 2018; Emadi and Baghernejad, 2014; Tripathi et al., 2015). This study does not introduce a new interpolation technique; its contribution lies in providing the first geostatistical characterisation of soil spatial variability for the hydromorphic mangrove soils of Diawling National Park, a Sahelian, seasonally flooded system that has received far less attention than humid tropical mangroves. The unusually severe, near pure-nugget short-range variability found here for pH, SOC and N offers a transferable diagnostic benchmark for similarly marginal, redox-dominated coastal soils, and a baseline dataset for future monitoring of this protected area. Against this background, the present study sets out to characterise the spatial variability of organic carbon (OC), pH, EC and total nitrogen, and to compare how the IDW and OK methods perform when mapping these parameters across the PND mangroves. The aim is to improve our understanding of the biogeochemical processes that operate in this arid setting and to supply baseline data for conserving and rehabilitating mangroves at the edge of their range. Fifty soil samples were collected from the surface beneath Avicennia germinans and Rhizophora racemosa within the study area, and a global positioning system (GPS) recorded the coordinates of each sampling point.

MATERIALS AND METHODS

Study area

The study was carried out in Diawling National Park (PND), in south-western Mauritania. The park lies between 16°35’00”N, 16°20’00” W and 16°05’00”N, 16°30’00” W. The site has considerable ecological and scientific importance because it marks the northern limit of the West African coastal mangroves, where the ecosystem persists in a desert to semi-arid climate marked by scarce rainfall, intense evaporation and high temperatures (Figure 1).

Soil sampling and laboratory analysis

Fifty soil samples were collected in January 2025 across the study area to capture the spatial variability of the soils’ physicochemical properties, from the surface layer (0–20 cm). Each sampling point was georeferenced by a handheld GPS device (Garmin 78) so that its coordinates could be recorded precisely and used in the subsequent spatial analyses (Table 1). The samples were taken with clean equipment, placed in suitable bags and transported to the laboratory, where they were air-dried, ground and sieved before analysis. The sampling followed a random design, with points placed at random locations within the parts of the site that were physically accessible. The sampling site, known as Birette, is located along the right-bank dike in the immediate vicinity of the Diama Dam and is fed by a natural marigot connecting the Senegal River to the Atlantic Ocean. This choice was dictated by site accessibility: the hydromorphic mangrove substrate is kept almost permanently flooded by this hydrological connection and forms a mosaic of submerged channels, soft mudflats and emergent banks that cannot be walked or traversed along a

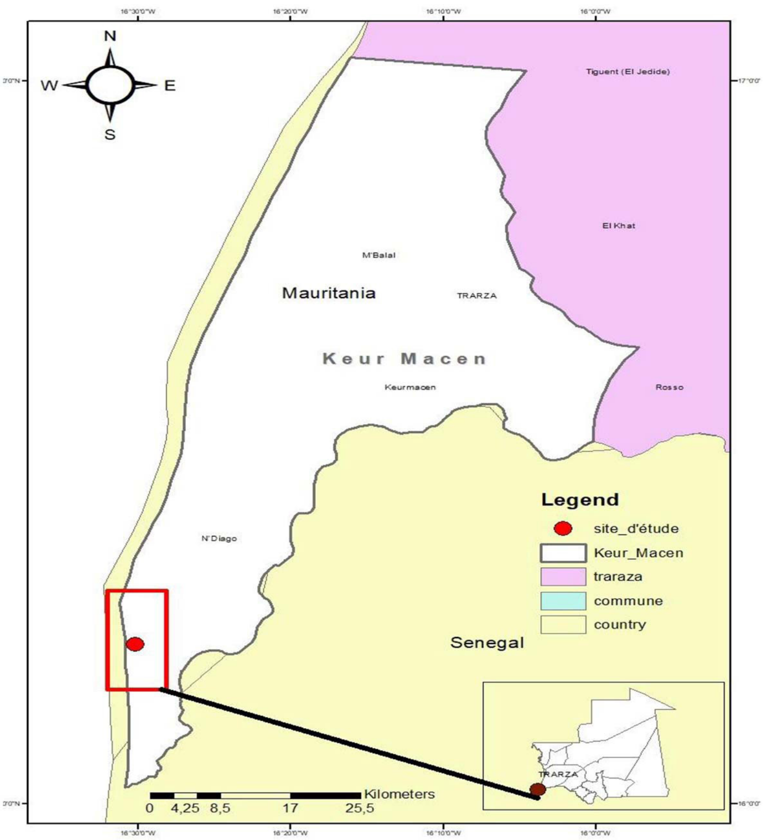

Figure 1. Map of the study area

Table 1. Geographic coordinates of the study area

Sample N°	Latitude Y (°N)	Longitude X (°W)
1	16.220615	16.502442
2	16.220668	16.502439
3	16.220678	16.502413
4	16.220632	16.502393
5	16.220655	16.502393
6	16.220692	16.502408
7	16.220666	16.502417
8	16.220697	16.502382
9	16.220705	16.502372
10	16.220713	16.502438
11	16.220718	16.502417
12	16.220706	16.502443
13	16.220688	16.502455
14	16.220681	16.502439
15	16.220665	16.502492
16	16.220531	16.502437
17	16.220683	16.502453
18	16.220631	16.502443
19	16.220688	16.502438
20	16.220681	16.502443
21	16.220684	16.502456
22	16.220619	16.502553
23	16.220717	16.502478
24	16.220719	16.502514
25	16.220697	16.502501
26	16.220673	16.502483
27	16.220705	16.502482
28	16.220734	16.502488
29	16.220723	16.502515
30	16.220739	16.502499
31	16.220739	16.502483
32	16.220683	16.502525
33	16.220757	16.502457
34	16.220724	16.502442
35	16.220721	16.502351
36	16.220753	16.502394
37	16.220934	16.502403
38	16.220832	16.502432
39	16.220825	16.502337
40	16.220844	16.502405
41	16.220839	16.502392
42	16.220878	16.502322
43	16.220741	16.502446
44	16.220798	16.502456
45	16.220798	16.502487
46	16.220769	16.502452
47	16.220763	16.502440
48	16.220782	16.502399
49	16.220702	16.502511
50	16.220674	16.502529

systematic transect. Sampling points were therefore randomly positioned wherever the substrate allowed safe access on foot beneath the canopy of Avicennia germinans, the locally dominant mangrove species at this site, and the less abundant Rhizophora racemosa. As a consequence, the 50 points are concentrated within a single mangrove, this fine-grained, locally dense spatial coverage is revisited when interpreting the semivariogram ranges and the cross-validation contrast between IDW and OK, and is discussed as a limitation.

Measurement of pH and electrical conductivity

For each sample, 10 g of soil was mixed with 50 mL of distilled water (1:5 w/v). The suspension was stirred on a magnetic stirrer for 1.5 h at room temperature and then left to stand so that the solid particles could settle. The supernatant was filtered through Whatman paper into a clean beaker. pH was measured on the filtrate with a previously calibrated pH meter, and electrical conductivity with a calibrated conductivity meter.

Soil organic carbon (SOC) analysis

Soil organic carbon was determined by the modified Walkley and Black method adapted for spectrophotometric reading (De Vos et al., 2007; Nelson and Sommers, 1982, 2018; Walinga et al., 1992; Walkley and Black, 1934). Samples that had been air-dried, ground and sieved to 2 mm were oxidised with potassium dichromate ($K_2Cr_2O_7$) in a strongly acidic medium, then digested with a potassium dichromate solution in the presence of concentrated sulfuric acid. After a controlled reaction time the solutions were diluted with distilled water to halt the reaction and prepare them for spectrophotometric reading. Absorbance was measured at 600 nm, the wavelength of maximum absorption for the complex formed when organic carbon is oxidised (Heanes, 1984). Organic carbon was then quantified from a calibration curve built with nine standard glucose solutions analysed under the same conditions. Absorbance (A) and carbon concentration (C, $g \cdot L^{-1}$) were strongly linear, following the regression equation:

$$A = 52.6654\ C + 0.0670 \quad (R^2 = 0.9971)$$

This regression equation was used to calculate the organic carbon content of the samples.

The digestion was heated to a controlled boil, following Anne (1945) and Dabin (1967, 1970), driving oxidation close to completion; the recovery factor of ~1.33 used for the original, unheated Walkley–Black procedure (Walkley and Black, 1934; De Vos et al., 2007) therefore does not apply here, as in other heated, calibration-curve adaptations (Heanes, 1984; Walinga et al., 1992)

Total soil nitrogen

Total nitrogen was determined by the Kjeldahl method, in which the sample is digested in concentrated sulfuric acid to form $(NH_4)_2SO_4$; the ammonia is then released with sodium bicarbonate and removed by steam (Bremner, 1960, 1996; Sáez-Plaza et al., 2013). One gram of ground soil was placed in a Pyrex flask with a pinch of selenium catalyst, 5 mL of 36 N H_2SO_4 and 5 drops of hydrogen peroxide. The mixture was heated to 300 °C for 3 to 10 minutes, left to cool for 15 minutes, and then made up with 20 mL of distilled water. Distillation was performed with 20 mL of NaOH (32%), 10 mL of H_3BO_3 (4%) and 30 mL of distilled water for 3 to 10 minutes. After adding 5 drops of red indicator, the distillate was titrated with H_2SO_4 N/50. Total nitrogen was calculated as %N = 0.028 × x, where x is the volume of acid used, given that 1 mL of H_2SO_4 N/50 corresponds to 0.28 mg of nitrogen. A reagent blank, carried through the same digestion and distillation steps but without soil, was titrated alongside the samples, and its volume was subtracted from each sample titration to correct for background ammonia, consistent with standard quality-control practice for the Kjeldahl method (Bremner, 1960; Sáez-Plaza et al., 2013).

Interpolation methods

Two interpolation methods were applied: ordinary kriging (OK) and inverse distance weighting (IDW). Both estimate unmeasured values of electrical conductivity (EC), pH, nitrogen (N) and SOC from the measured data. Correlation coefficients and performance criteria were used to identify the method best suited to the study area. All field coordinates were recorded using the WGS 1984 / UTM projection system. Statistical calculations were performed using Jamovi 2.7 and Microsoft Excel, while geostatistical analysis and the generation of interpolation maps were carried out using ArcGIS 10.8. The sampling point layer was imported into ArcGIS as a shapefile, and values for physicochemical parameters (EC, pH, SOC, and N) were joined to the point features. Interpolation maps based on IDW and ordinary kriging were generated for the entire study area using a 0.09 m² grid cell size. For IDW, the weighting exponent was set to β = 2, and a variable search radius encompassing the 12 nearest neighbors was used, without a maximum distance constraint, in accordance with the parameters most commonly adopted for these types of soil properties (Abidine et al., 2018; Bhunia et al., 2018; Seyedmohammadi et al., 2016). For ordinary kriging, experimental semivariograms were first calculated for each property and then visually fitted by selecting an appropriate theoretical model (spherical, exponential, or Gaussian) and manually adjusting the nugget effect, sill, and range until the modeled curve accurately reproduced the shape of the experimental semivariogram; this classic manual fitting procedure is standard practice in applied geostatistics (Webster and Oliver, 2007; Tripathi et al., 2015). The resulting prediction maps were exported at a resolution of 400 dpi to ensure high quality.

OK method

Ordinary kriging is among the most widely used interpolation techniques (Mousavifard et al., 2013; Poshtmasari et al., 2012). It estimates values over an area surrounding each sampled point (Abidine et al., 2018; Pang et al., 2011; Seyedmohammadi et al., 2016; Tripathi et al., 2015). The semivariogram is expressed as follows:

$$\gamma(h) = \frac{1}{2N(h)} \sum_{i=}^{N(h)} [Z(x_i) - Z(x_i + h]^2 \quad (1)$$

where: $\gamma(h)$ is the semi-variance, $N(h)$ the number of data pairs separated by a given distance, h the lag distance, Z the measured value of the soil property and x the position of the sample.

IDW method

Inverse distance weighting is one of the interpolation methods commonly used in soil science (Bhunia et al., 2018; Abidine et al., 2018; Robinson and Metternicht, 2006; Seyedmohammadi et al., 2016). Its estimates rely on known values in the surrounding area (Equation 2), with each interpolation weight set as the inverse of the distance to the prediction point.

$$Z(x_0) = \frac{\sum_{i=}^{n} \frac{x_i}{h_{ij}^{\beta}}}{\sum_{i=1}^{n} \frac{1}{h_{ij}^{\beta}}} \quad (2)$$

where: $Z(x_0)$ is the interpolated value, n the total number of sample points, x_i the measured value, $h\_(ij)$ the distance between the interpolated and measured values, and β the weighting power ($\beta = 2$).

This value of β was fixed a priori rather than optimised by minimising the cross-validation error, following the default setting most commonly adopted for soil properties of this kind (Abidine et al., 2018; Bhunia et al., 2018; Seyedmohammadi et al., 2016).

Performance evaluation criteria

Cross-validation followed a leave-one-out procedure, in which each point's re-estimated value was compared with its measured value, following Tripathi et al. (2015). Six standard statistical metrics were used to assess the predictive accuracy of the models: mean error (ME), root mean square error (RMSE), correlation coefficient (R), mean standardised error (MSE), standardised root mean square error (RMSSE) and average standard error (ASE). Performance was evaluated with the following equations:

$$ME = \sum_{i=1}^{n} \frac{[z^*(x) - z(x)]^2}{n} \quad (3)$$

$$RMSE = \sqrt{\sum_{i=1}^{n} \frac{[z^*(x) - z(x)]^2}{n}} \quad (4)$$

$$ASE = \sqrt{\frac{\sum_{i=1}^{n} \sigma^*(x)}{n}} \quad (5)$$

$$MSE = \frac{\sum_{i=1}^{n} \frac{Z^*(x) - Z(x)}{\sigma^*(x)}}{n} \quad (6)$$

$$RMSSE = \sqrt{\frac{\sum_{i}^{n} [\frac{\{z^*(x) - z(x)\}^2}{\sigma^*(x)}]^2}{n}} \quad (7)$$

where: $z(x)$ is a measured value, $z^*(x)$ a predicted value and $\sigma^*(x)$ the variance of the prediction.

The formulations of Equation 3 (ME) and Equation 7 (RMSSE), follow exactly those given by Tripathi et al. (2015).

$$R = \sqrt{1 - \left[\frac{(\sum_{i=1}^{n}(y_i - y_i')^2}{\sum_{i=1}^{n}(y_i - \bar{y_i})^2}\right]} \quad (8)$$

where: y_i is the observed value, $y_{i'}$ the predicted value, $\bar{y}_i$ the mean of the observed values and n the number of observations.

RESULTS AND DISCUSSION

Descriptive statistics

The descriptive statistics (Table 2) give a mean pH of 7.22 ± 0.738 (CV = 10.2%), with values between 6.12 and 8.66. This neutral to slightly alkaline range is typical of hydromorphic mangrove soils that undergo intense redox cycling, in which the alternation of anaerobic flooding and oxidising emersion creates short-distance pH gradients (Dookie et al., 2024; Zheng et al., 2025). Under permanent flooding, sulfate reduction releases OH^- ions that raise pH, whereas the oxidation of sulfides produces acidic protons. The observed interval [6.12–8.66] reflects this redox dynamic, which is characteristic of hydromorphic mangrove soils (Krauss et al., 2008). The moderate positive skewness ($g_1 = +0.570$) and the kurtosis (-0.996) point to a distribution without marked deviation, a condition that favours the use of interpolation methods (Ahmed et al., 2017; Bhunia et al., 2018).

EC is the most variable parameter (μ = 2.52 mS/cm, CV = 38.4%, range (0.38–3.91) mS/cm; Table 2). In hydromorphic mangrove soils, interstitial salinity reflects a balance between freshwater inputs from the Senegal River, tidal seawater intrusion and concentration through evapotranspiration during the dry season (Ngom et al., 2016). The high heterogeneity recorded here (CV = 38.4%) is consistent with such environments; Tripathi et al. (2015) report comparable CV values (30–45%) for EC in flooded saline coastal soils of India and attribute this variability to local hydraulic gradients between permanently flooded and seasonally submerged areas. The negative skewness ($g_1 = -0.424$) indicates a distribution shifted toward high values, a sign of active salinisation amplified by the reduced freshwater supply that has followed the closure of the Diama Dam in 1986 (Nuscia Taïbi et al., 2007). For comparison, Abidine et al. (2018), working in the same

Table 2. Descriptive statistics of physicochemical parameters

Parameter	pH	EC (mS cm^{-1})	SOC (%)	N (%)
N	50	50	50	50
Mean	7.22	2.52	0.680	0.0423
Median	7.06	2.59	0.611	0.0426
Standard deviation	0.738	0.968	0.244	0.00694
Minimum	6.12	0.380	0.311	0.0294
Maximum	8.66	3.91	1.18	0.0544
CV%	10.2	38.4	35.9	16.4
Skewness	0.570	-0.424	0.384	-0.132
Kurtosis	-0.996	-0.816	-0.907	-0.880

park but on dry, non-flooded soils, report a much higher mean EC of 11.48 mS/cm; this confirms that the constantly flooded, hydromorphic character of mangrove soils buffers salinity through interstitial dilution.

Soil organic carbon averaged 0.680 ± 0.244% (CV = 35.9%; Table 2). Although hydromorphic mangrove soils are recognised as important carbon sinks worldwide, the values found here remain below those of humid tropical mangroves (1–5%). The combined saline and water stress that affects Sahelian mangroves at the northern limit of their range accounts for this difference (Wu et al., 2025; Xia et al., 2022). In such settings, high salinity suppresses microbial activity and slows the build-up of organic matter, even though the anoxic conditions of permanent flooding tend to preserve it (Dookie et al., 2024). Total nitrogen is the most homogeneous variable (μ = 0.0423%, CV = 16.4%, g_1 = -0.132; Table 2); its mean and median almost coincide, which indicates a symmetrical distribution. This pattern reflects the close biogeochemical coupling between nitrogen and organic matter in a slowly decomposing, anoxic hydromorphic soil (Hu et al., 2024; Ray et al., 2023).

Semivariogram analysis and spatial structure of soil properties

Before ordinary kriging was performed, experimental semivariograms were computed for EC, pH, SOC and N and fitted visually with theoretical models (exponential, spherical or Gaussian) by manually adjusting the nugget, sill and range until the modelled curve reproduced the shape of the experimental semivariogram; the residual sum of squares between the experimental and modelled semivariance served as the goodness-of-fit criterion to guide model selection. The fitted nugget (C0), sill (C0+C), range and nugget-to-sill proportion are reported in Table 3.

The four properties are best described by contrasting theoretical models, exponential for EC and N, spherical for pH and Gaussian for SOC, a diversity of model types commonly reported for coastal and saline soils elsewhere (Tripathi et al., 2015; Sahbeni and Székely, 2022). The fitted ranges are short, between 3.56 m for N and 14.80 m for SOC, showing that spatial autocorrelation decays within a few metres in this hydromorphic environment, well inside the extent of the sampling grid (Trangmar et al., 1986). Sample pairs separated by larger distances therefore contribute essentially uncorrelated information to the kriging system, a structural constraint that helps explain the contrasting cross-validation results obtained with ordinary kriging (Table 4).

Electrical conductivity shows a nugget-to-sill ratio of 0.7569 (75.7%), a value that lies within the conventional 0–100% scale, right at the boundary of the moderate and weak classes of Cambardella et al. (1994), and indicates weak spatial dependence; only a small fraction of its total variance is spatially structured, the remainder reflecting unresolved short-range heterogeneity. This is consistent with the intermediate, but clearly imperfect, cross-validation performance of OK for this variable (R = 0.647; Table 4) and falls in the same range as the weak-to-moderate dependence reported for EC, or its model residuals, in other saline and seasonally flooded soils (Tripathi et al., 2015; Sahbeni and Székely, 2022; Emadi and Baghernejad, 2014; Kaya et al., 2022).

For pH and SOC, the nugget exceeds the sill (ratios of 5.3158 and 2.9924), an unrealistic configuration that typically signals an absence of a

Table 3. Semi-variogram model parameters adjusted to the physico-chemical properties of soils

Soil property	Fitted model	Range (m)	Nugget (C0)	Sill (C0+C)	Proportion (C0/(C0+C))
EC	Exponential	14.119	0.460	0.608	0.7569
pH	Spherical	10.168	0.498	0.094	5.3158
SOC	Gaussian	14.797	4.876E-06	1.630E-06	2.9924
N	Exponential	3.560	4.883E-05	2.983E-06	16.3692

clear plateau in the experimental semivariogram. This is functionally equivalent to a pure nugget effect: variation is essentially random at the scale of the sampling grid. Such outcomes are not unusual, similar pure nugget effects have been reported for other soil properties in comparable field studies (Swafo and Dlamini, 2023; Siqueira et al., 2014), often linked to sampling resolution that is too coarse to capture fine-scale variability. This fits with evidence that redox status in flooded soils is structured at the microsite scale rather than at the scale of typical soil cores (Lacroix et al., 2023), meaning nearby cores can fall on opposite sides of a microsite boundary and generate variance below the survey's minimum sampling distance. This explains the near-flat semivariograms for pH and SOC (Figure 2) and the poor cross-validation results for ordinary kriging (R = 0.091 for pH, R = 0.445 for SOC; Table 4), both weaker than the moderate spatial dependence found for mangrove SOC in Thailand (Chaikaew and Chavanich, 2017).

Total nitrogen shows the same pattern in its most extreme form, with a nugget-to-sill ratio of 16.3692, that is, a fitted nugget nearly sixteen and a half times larger than the fitted sill. As with pH and SOC, this value falls outside the conventional 0–100% scale and is best read as a strong indicator of an unstable model fit driven by an almost complete absence of structured spatial variance (Webster and Oliver, 2007). The shortest range of the four properties (3.56 m) reinforces this diagnosis of an almost purely random spatial signal for N. Yet OK still performs remarkably well for this variable in cross-validation (R = 0.989; Table 4), an apparent paradox that is resolved by the very low absolute variability of N (CV = 16.4%, the lowest of the four properties; Table 2): even a kriging system built on a semivariogram with no usable structure behaves locally like a simple moving average, and when the underlying variance is small, such an average still reproduces the narrow range of measured values with high accuracy. An extremely high, ill-defined nugget-to-sill ratio therefore does not necessarily translate into poor cross-validation statistics. Taken together, these results show that unstructured short-range variability, rather than the intrinsic nature of each property, governs the comparative performance of OK across the four properties (Khosravi et al., 2016; Poshtmasari et al., 2012).

Comparison of the IDW and OK methods

Table 4 shows IDW clearly outperforming OK for all four parameters, with correlation coefficients near 1 (R = 0.9998–0.99994) and negligible mean errors, indicating no systematic bias. This matches Abidine et al. (2018), who found the same advantage for IDW in different (dry) soils at the same site, suggesting IDW's superiority depends more on data structure than soil type. OK performs unevenly across properties: well for N (R = 0.989, despite the most extreme nugget-to-sill ratio of the four properties, moderately for EC (R = 0.647), poorly for SOC (R = 0.445), and very poorly for pH (R = 0.091. This ordering alone would suggest, showing that cross-validation accuracy and the nugget-to-sill diagnostic don't always align perfectly. This pattern reflects strong short-range variability typical of hydromorphic, redox-affected soils, which disadvantages OK (Poshtmasari et al., 2012; Tripathi et al., 2015; Sahbeni and Székely, 2022). However, with 50 points over a small area, IDW's inverse-square weighting means each left-out point in cross-validation is predicted almost entirely by its closest near-duplicate neighbour rather than a true areal average. This artificially inflates IDW's accuracy due to the sampling design itself, not the method's intrinsic quality, an effect much less pronounced for OK, which relies on a globally fitted variogram rather than the single nearest point. The ASE value close to one for EC (IDW = 0.9651) indicates a sound calibration of the predictive uncertainty. The lower ASE values for SOC (0.2424) and N (0.0069) point to

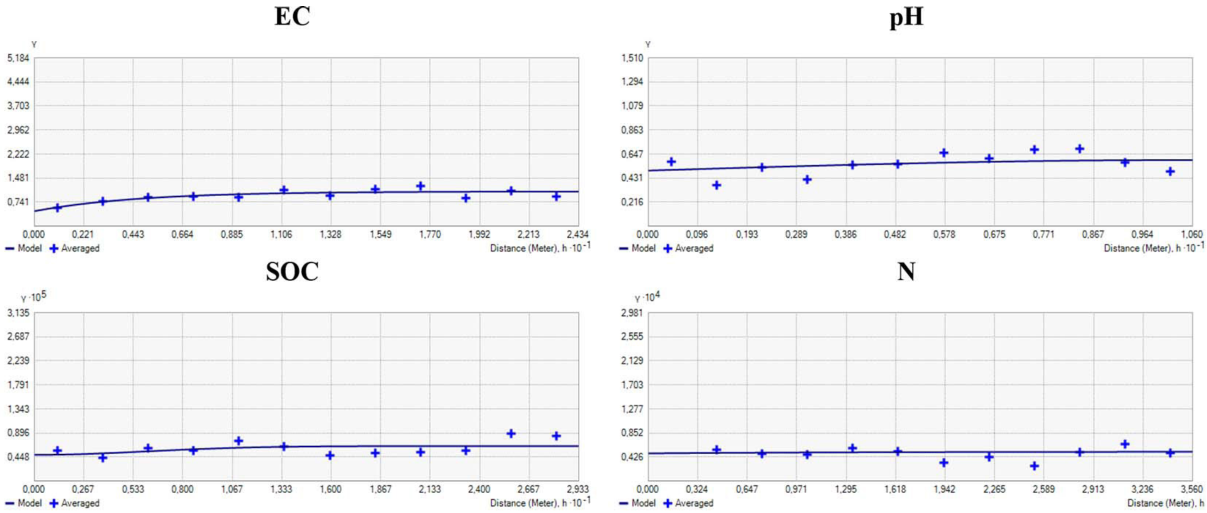

Figure 2. Experimental semivariograms and fitted theoretical models for EC, pH, SOC and N

Table 4. Metrics for evaluating interpolation performance

Setting	Method	ME	RMSE	R	MSE	RMSSE	ASE
CE	IDW	6.47 E-05	0.008041	0.99994	7.23E-05	6.7E-05	0.965093
	OK	0.38654	0.62172	0.64743	-0.0575	0.73371	0.52682
pH	IDW	0.00046	0.0214475	0.9992534	-0.000473	0.00063	0.7301186
	OK	0.48622	0.6973	0.09122	0.5479	2.17034	0.22403
CO	IDW	2E-05	0.005	0.9996	0.0003	0.0001	0.2424
	OK	0.03848	0.19617	0.44497	0.49181	0.45956	0.08374
N	IDW	1E-08	0.0001	0.9998	0.121	0.0003	0.0069
	OK	3E-06	0.0016	0.9894	-0.582	0.0926	0.0054

an underestimation of the predictive variance, a known feature of IDW, which is a deterministic method and provides no error estimate (Robinson and Metternicht, 2006). Ahmed et al. (2017), note the same limitation when mapping pH in Pakistani orchards. Even so, the six independent criteria (ME, RMSE, R, MSE, RMSSE, ASE) agree with one another, which confirms the robustness of the results: IDW is consistently better than, or equal to, OK across all criteria and parameters, the only exception being N, where the two methods are comparable.

IDW interpolation maps

The IDW maps (Figure 3) reveal an organised spatial pattern in the hydromorphic soil properties. Electrical conductivity follows a bipolar distribution: high values (2.93–3.30 mS/cm) concentrate in the northern sector, where weak hydraulic connectivity allows evapotranspiration to concentrate salts, while low values (1.18–1.70 mS/cm) occur where flooding and tides renew the water frequently. This pattern mirrors the flooding gradient of mangrove hydromorphic soils, in which the frequency of submersion controls interstitial salinity (Ngom et al., 2016; Tripathi et al., 2015). pH forms a fine-scale mosaic, with alkaline zones (pH 7.83–8.65) in evaporitic depressions where carbonates precipitate and more acidic zones (6.12–6.76) in microsites of active sulfate reduction. Such a mosaic is a characteristic signature of these soils, where redox cycles governed by the depth of the interstitial water table control pH variability (Dookie et al., 2024; Zheng et al., 2025). Soil organic carbon and total nitrogen, for their part, reach higher concentrations in areas of prolonged flooding, in keeping with the role of anoxia in preserving organic matter in hydromorphic environments (Xia et al., 2022; Yin et al., 2023).

OK interpolation maps

Comparing the OK maps (Figure 4) with the IDW maps (Figure 3) reproduces the performance

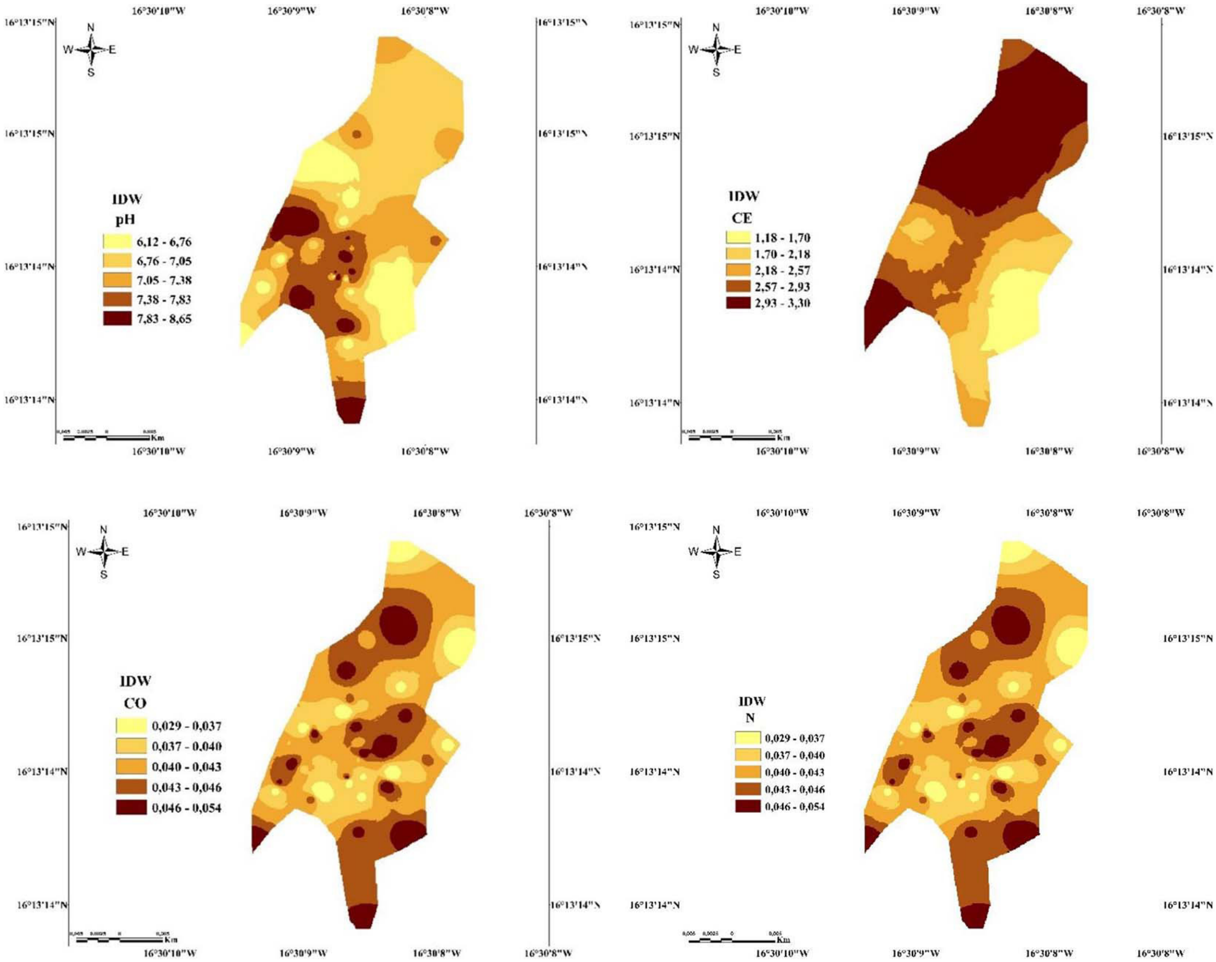

Figure 3. IDW interpolation maps for pH, EC, SOC, and N

contrasts of Table 4. For N the two methods agree, in line with their comparable scores. For EC, OK captures the broad spatial trends but smooths out the local heterogeneity of the hydromorphic environment. These fine gradients matter ecologically in soils subject to wetting and drying cycles, yet the geostatistical smoothing of OK partly hides them. For pH, OK narrows the range to (6.82–7.77), against (6.12–8.65) for IDW, and introduces angular structures linked to the strong short-range variability of the environment. In a hydromorphic mangrove soil, where short-range pH gradients govern the activity of anaerobic microbial communities and sulfate reduction, this loss of detail is especially damaging for ecological interpretation (Dookie et al., 2024). For SOC, the OK map creates artificial discontinuities in the northern sector that are absent from the IDW map, again a direct consequence of the strong short-range heterogeneity of the soil. Such artefacts, already documented by Emadi and Baghernejad (2014) for coastal saline soils of similar variability, make OK unsuitable for quantifying SOC stocks here. The mapped physicochemical gradients could also have ecophysiological implications for Avicennia germinans and Rhizophora racemosa within the study area, however, this study did not include direct measurements of vegetation cover, plant physiology or porewater chemistry, so the following associations are presented as hypotheses consistent with findings reported elsewhere for these species, rather than as conclusions established at this site. The high EC values of the northern sector (2.93–3.30 mS/cm) fall within a range that, in other stands of Avicennia and Rhizophora, has been associated with salt-exclusion and leaf-excretion mechanisms that lower stomatal conductance and water-use efficiency (Madrid et al., 2014; Muller et al., 2009); whether the same response occurs at this site remains to be verified by direct measurement. Likewise, the acidic pH zones (6.12–6.76) linked to sulfate reduction coincide with conditions that, in comparable settings, limit nutrient

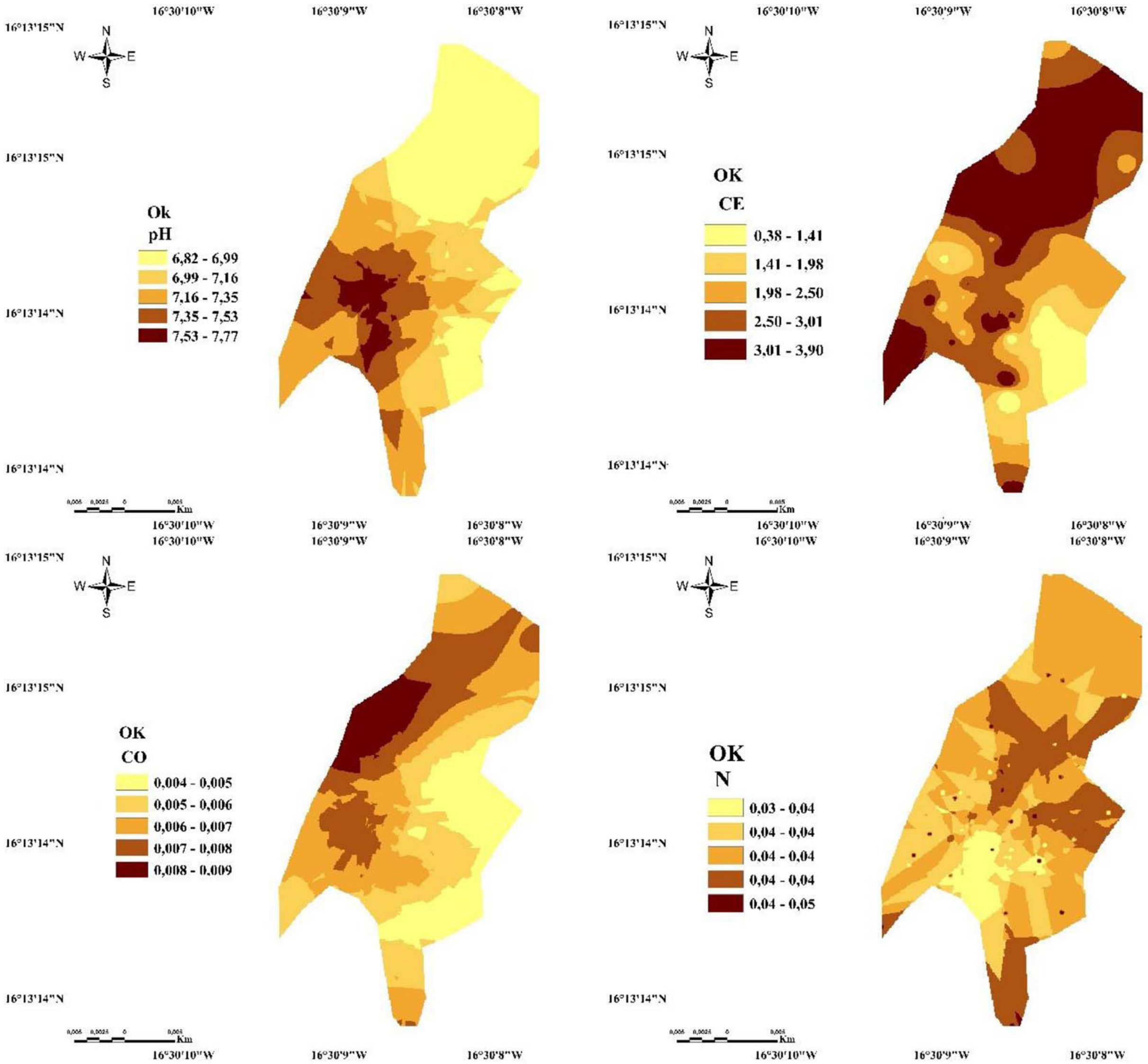

Figure 4. OK interpolation maps for pH, EC, SOC, and N

availability and hinder root development through sulfide phytotoxicity (Dookie et al., 2024; Krauss et al., 2008), while the prolonged-flooding areas rich in organic carbon and nitrogen correspond to conditions generally regarded as favourable for biomass production and blue-carbon storage, since anoxia tends to stabilise organic matter (Hu et al., 2024; Xia et al., 2022). These spatial associations illustrate how the mapped edaphic gradients could plausibly relate to the ecological functioning of mangrove species in this Sahelian context (Meera et al., 2023; Zhu et al., 2011), and they motivate a dedicated field assessment of vegetation and physiology as a priority for future work at this site. Overall, the advantage of IDW in this hydromorphic environment stems from the strong short-range variability that redox processes create; the resulting unstructured heterogeneity systematically undermines ordinary kriging (Khosravi et al., 2016; Zarco-Perelló and Simões, 2017). Several recent studies in settings as varied as desert national parks and coastal urban areas confirm this dominance of IDW under Mauritanian soil conditions (Abidine et al., 2023, 2024). The result shows that the choice of interpolation method cannot be divorced from the pedological processes that govern spatial variability. In hydromorphic soils subject to intense redox cycling, unstructured short-range variability is inherently high, which favours deterministic methods such as IDW over geostatistical approaches that require well-defined spatial autocorrelation (Robinson and Metternicht, 2006; Sahbeni and Székely, 2022).

CONCLUSIONS

This study shows that the hydromorphic mangrove soils of Diawling National Park display strong spatial variability in their physicochemical properties, controlled by the hydraulic gradients and redox processes typical of this Sahelian setting. Organic carbon contents, lower than those of humid tropical mangroves, reflect the saline and water stress that marks these marginal ecosystems. For mapping edaphic properties under such strong short-range heterogeneity, IDW proves clearly superior to ordinary kriging, which confirms that the choice of interpolation method must follow an understanding of the underlying pedological processes. Semivariogram modelling corroborates this conclusion: EC shows weak spatial dependence (nugget-to-sill ratio = 0.7569), while pH, SOC and N show a fitted nugget exceeding the fitted sill, a pattern functionally equivalent to a pure nugget effect, confirming that unstructured short-range variability, rather than the intrinsic nature of the soil, drives the comparative performance of the two interpolation methods in this hydromorphic context. Some limitations should be acknowledged: the sampling was concentrated within a single mangrove stand, which constrains the resolved semivariogram ranges and may inflate IDW's cross-validation accuracy; the IDW weighting power was fixed rather than optimised, and IDW provides no native uncertainty estimate, unlike OK; and the ecological interpretations remain working hypotheses pending direct field measurement. These results provide a methodological reference for mapping edaphic properties in this type of hydromorphic mangrove microhabitat in the PND and pave the way for the assessment of blue carbon stocks and the analysis of how these mangroves respond ecophysiologically to the mapped edaphic gradients.

REFERENCES

1. Abidine, M. M., Baba, M. L., Cherif, S. M. A., Beddi, Z. A., Dallahi, Y., Sidine, M. O., Soulé, A., Vadel, A. (2024). Mapping soil electrical conductivity as an indicator of soil salinity in the city of Nouakchott (Mauritania). *Geographia Technica, 19*(2), 227–236. https://doi.org/10.21163/GT_2024.192.18
2. Abidine, M. M., Cheikh, L. M., Dallahi, Y., Baba, M. L., Mahmoud, E. W. M., Soulé, A., Vadel, A. (2023). The study of the germination behavior of forage species on substrates taken from the soil of Awleigatt National Park in Mauritania. *Ecological Engineering & Environmental Technology, 24*(6), 257–269. https://doi.org/10.12912/27197050/168453
3. Abidine, M. M. O., Aboudi, A. El, Kebd, A., Aloueimine, B. B., Dallahi, Y., Soulé, A., Vadel, A. (2018). Modeling the spatial variability of the electrical conductivity of the soil using different spatial interpolation methods: case of the Dawling National Park in Mauritania. *Geographia Technica, 13*(2), 1-11. https://doi.org/10.21163/GT_2018.132.01
4. Ahmed, H., Siddique, M. T., Iqbal, M., Hussain, F. (2017). Comparative study of interpolation methods for mapping soil pH in the apple orchards of Murree, Pakistan. *Soil & Environment, 36*(1), 70–76.
5. Anne, P. (1945). The rapid determination of organic carbon in soils. *Annales Agronomiques, 15*, 161–172.
6. Bernal, B., Mitsch, W. J. (2012). Comparing carbon sequestration in temperate freshwater wetland communities. *Global Change Biology, 18*(5), 1636–1647. https://doi.org/10.1111/j.1365-2486.2011.02619.x
7. Bhunia, G. S., Shit, P. K., Maiti, R. (2018). Comparison of GIS-based interpolation methods for spatial distribution of soil organic carbon (SOC). *Journal of the Saudi Society of Agricultural Sciences, 17*(2), 114–126. https://doi.org/10.1016/j.jssas.2016.02.001
8. Bremner, J. M. (1960). Determination of nitrogen in soil by the Kjeldahl method. *The Journal of Agricultural Science, 55*(1), 11–33. https://doi.org/10.1017/S0021859600021572
9. Bremner, J. M. (1996). *Total nitrogen*. In Methods of Soil Analysis, Part 2: Chemical and Microbiological Properties (pp. 1149–1178). https://doi.org/10.2134/agronmonogr9.2.c32
10. Cambardella, C. A., Moorman, T. B., Novak, J. M., Parkin, T. B., Karlen, D. L., Turco, R. F., Konopka, A. E. (1994). Field-scale variability of soil properties in central Iowa soils. *Soil Science Society of America Journal, 58*(5), 1501–1511. https://doi.org/10.2136/sssaj1994.03615995005800050033x
11. Chaikaew, P., Chavanich, S. (2017). Spatial variability and relationship of mangrove soil organic matter to organic carbon. *Applied and Environmental Soil Science*, 2017, https://doi.org/10.1155/2017/4010381
12. Chowdhury, A., Naz, A., Dasgupta, R., Maiti, S. K. (2023). Blue carbon: comparison of chronosequences from Avicennia marina plantation and *Porteresia coarctata* dominated mudflat, at the world's largest mangrove wetland. *Sustainability, 15*(1), 368. https://doi.org/10.3390/su15010368
13. Cui, L., Sun, H., Du, X., Feng, W., Wang, Y., Zhang, J., Jiang, J. (2021). Dynamics of labile soil organic carbon during the development of

mangrove and salt marsh ecosystems. *Ecological Indicators, 129*, 107875. https://doi.org/10.1016/j.ecolind.2021.107875

14. Dabin, B. (1967). *Application of automated dosing to soil analysis.* Horizon.Documentation.Ird.Fr, Cah. ORS. T 0. M. series Pedology Vol. N" 3 - 1967
15. Dabin, B. (1970). Determination of total organic carbon. In: Analysis of organic matter in soils. Https://Horizon.Documentation.Ird.Fr/Exl-Doc/Pleins_textes_5/B_fdi_04-05/05490.Pdf, 1/3.
16. De Vos, B., Lettens, S., Muys, B., Deckers, J. A. (2007). Walkley-Black analysis of forest soil organic carbon: recovery, limitations and uncertainty. *Soil Use and Management, 23*(3), 221–229. https://doi.org/10.1111/j.1475-2743.2007.00084.x
17. Dookie, S., Jaikishun, S., Ansari, A. A. (2024). Interactions between mangrove soil, water, and microbes in degraded, natural, and restored tropical coastline ecosystems. *Biodiversity, 25*(1), 21–41. https://doi.org/10.1080/14888386.2023.2301283
18. Emadi, M., Baghernejad, M. (2014). Comparison of spatial interpolation techniques for mapping soil pH and salinity in agricultural coastal areas, northern Iran. *Archives of Agronomy and Soil Science, 60*(9), 1315-1327. https://doi.org/10.1080/03650340.2014.880837
19. Feng, J., Cui, X., Zhou, J., Wang, L., Zhu, X., Lin, G. (2019). Effects of exotic and native mangrove forests plantation on soil organic carbon, nitrogen, and phosphorus contents and pools in Leizhou, China. *Catena, 180*, 1–7. https://doi.org/10.1016/j.catena.2019.04.018
20. Gao, Y., Zhou, J., Wang, L., Guo, J., Feng, J., Wu, H., Lin, G. (2019). Distribution patterns and controlling factors for the soil organic carbon in four mangrove forests of China. *Global Ecology and Conservation, 17*, e00575. https://doi.org/10.1016/j.gecco.2019.e00575
21. Heanes, D. L. (1984). Determination of total organic carbon in soils by an improved chromic acid digestion and spectrophotometric procedure. *Communications in Soil Science and Plant Analysis, 15*(10), 1191–1213. https://doi.org/10.1080/00103628409367551
22. Herbert, E. R., Schubauer-Berigan, J., Craft, C. B. (2018). Differential effects of chronic and acute simulated seawater intrusion on tidal freshwater marsh carbon cycling. *Biogeochemistry, 138*(2), 137–154. https://doi.org/10.1007/s10533-018-0436-z
23. Hu, J., Pradit, S., Loh, P. S., Chen, Z., Guo, C., Le, T. P. Q., Oeurng, C., Sok, T., Mohamed, C. A. R., Lee, C. W., Bong, C. W., Lu, X., Anshari, G. Z., Kandasamy, S., Wang, J. (2024). Storage and dynamics of soil organic carbon in allochthonous-dominated and nitrogen-limited natural and planted mangrove forests in southern Thailand. *Marine Pollution Bulletin, 200*, 116064. https://doi.org/10.1016/j.marpolbul.2024.116064
24. Kaya, F., Schillaci, C., Keshavarzi, A., Başayiğit, L. (2022). Predictive mapping of electrical conductivity and assessment of soil salinity in a Western Türkiye alluvial plain. *Land, 11*(12), 2148. https://doi.org/10.3390/land11122148
25. Khosravi, H., Karimi, K., Nakhaee Nejadfard, S., Mesbahzadeh, T. (2016). Investigation of spatial structure of groundwater quality using geostatistical approach in Mehran Plain, Iran. *Pollution, 2*(1), 57–65. https://doi.org/10.7508/pj.2016.01.006
26. Krauss, K. W., Lovelock, C. E., McKee, K. L., López-Hoffman, L., Ewe, S. M. L., Sousa, W. P. (2008). Environmental drivers in mangrove establishment and early development: a review. *Aquatic Botany, 89*(2), 105–127. https://doi.org/10.1016/j.aquabot.2007.12.014
27. Lacroix, E. M., Aeppli, M., Boye, K., Brodie, E., Fendorf, S., Keiluweit, M., Naughton, H. R., Noël, V., Sihi, D. (2023). Consider the anoxic microsite: acknowledging and appreciating spatiotemporal redox heterogeneity in soils and sediments. *ACS Earth and Space Chemistry, 7*(9), 1592–1609. https://doi.org/10.1021/acsearthspacechem.3c00032
28. Lal, R., Kimble, J. M., Stewart, B. A., Eswaran, H. (1999). *Global climate change and pedogenic carbonates*. Lewis Publishers, Boca Raton, FL.
29. Luo, Z., Feng, W., Luo, Y., Baldock, J., Wang, E. (2017). Soil organic carbon dynamics jointly controlled by climate, carbon inputs, soil properties and soil carbon fractions. *Global Change Biology, 23*(10), 4430-4439. https://doi.org/10.1111/gcb.13767
30. Madrid, E. N., Armitage, A. R., Lopez-Portillo, J. (2014). Avicennia germinans (black mangrove) vessel architecture is linked to chilling and salinity tolerance in the Gulf of Mexico. *Frontiers in Plant Science, 5*, 503. https://doi.org/10.3389/fpls.2014.00503
31. Maietta, C. E., Monsaint-Queeney, V., Wood, L., Baldwin, A. H., Yarwood, S. A. (2020). Plant litter amendments in restored wetland soils altered microbial communities more than clay additions. *Soil Biology and Biochemistry, 147*, 107846. https://doi.org/10.1016/j.soilbio.2020.107846
32. Meera, S. P., Bhattacharyya, M., Kumar, A. (2023). Dynamics of mangrove functional traits under osmotic and oxidative stresses. *Plant Growth Regulation, 101*(2), 285–306. https://doi.org/10.1007/s10725-023-01034-9
33. Mousavifard, S. M., Momtaz, H., Sepehr, E., Davatgar, N., Sadaghiani, M. H. R. (2013). Determining and mapping some soil physico-chemical properties using geostatistical and GIS techniques in the Naqade region, Iran. *Archives of Agronomy and Soil Science, 59*(11), 1573–1589. https://doi.org/10.1080/03650340.2012.740556
34. Muller, E., Lambs, L., Fromard, F. (2009). Variations

in water use by a mature mangrove of Avicennia germinans, French Guiana. *Annals of Forest Science, 66*(8), 803. https://doi.org/10.1051/forest/2009079

35. Murdiyarso, D., Purbopuspito, J., Kauffman, J. B., Warren, M. W., Sasmito, S. D., Donato, D. C., Manuri, S., Krisnawati, H., Taberima, S., Kurnianto, S. (2015). The potential of Indonesian mangrove forests for global climate change mitigation. *Nature Climate Change, 5*(12), 1089–1092. https://doi.org/10.1038/nclimate2734
36. Nelson, D. W., Sommers, L. E. (1982). *Total carbon, organic carbon, and organic matter*. In Methods of Soil Analysis, Part 2 (pp. 539–579). https://doi.org/10.2134/agronmonogr9.2.2ed.c29
37. Nelson, D. W., Sommers, L. E. (2018). *Total carbon, organic carbon, and organic matter*. In Methods of Soil Analysis, Part 3: Chemical Methods (pp. 961–1010). https://doi.org/10.2136/sssabookser5.3.c34
38. Ngom, F. D., Tweed, S., Bader, J. C., Saos, J. L., Malou, R., Leduc, C., Leblanc, M. (2016). Rapid evolution of water resources in the Senegal delta. *Global and Planetary Change, 144*, 34–47. https://doi.org/10.1016/j.gloplacha.2016.07.002
39. Nuscia Taïbi, A., el Habib Barry, M., Jolivel, M., Ballouche, A., Lemine Ould Baba, M., Moguedet, G., Lemine Ould, M. (2007). Enjeux et impacts des barrages de Diama (Mauritanie) et Arzal (France) : des contextes socio-économiques et environnementaux différents pour de mêmes conséquences. *Norois,* (203), 51-66. https://doi.org/10.4000/norois.1536
40. Pang, S., Li, T. X., Zhang, X. F., Wang, Y. D., Yu, H. Y. (2011). Spatial variability of cropland lead and its influencing factors: a case study in Shuangliu county, Sichuan province, China. *Geoderma, 162*(3–4), 223–230. https://doi.org/10.1016/j.geoderma.2011.01.002
41. Poshtmasari, H. K., Tahmasebi Sarvestani, Z., Kamkar, B., Shataei, S., Sadeghi, S. (2012). Comparison of interpolation methods for estimating pH and EC in agricultural fields of Golestan province (northern Iran). *International Journal of Agriculture and Crop Sciences, 4*(4), 157–167.
42. Ray, R., Suwa, R., Miyajima, T., Munar, J., Yoshikai, M., San Diego-McGlone, M. L., Nadaoka, K. (2023). Sedimentary blue carbon dynamics based on chronosequential observations in a tropical restored mangrove forest. *Biogeosciences, 20*(4), 911–928. https://doi.org/10.5194/bg-20-911-2023
43. Robinson, T. P., Metternicht, G. (2006). Testing the performance of spatial interpolation techniques for mapping soil properties. *Computers and Electronics in Agriculture, 50*(2), 97–108. https://doi.org/10.1016/j.compag.2005.07.003
44. Sáez-Plaza, P., Navas, M. J., Wybraniec, S., Michałowski, T., Asuero, A. G. (2013). An overview of the Kjeldahl method of nitrogen determination. Part II. Sample preparation, working scale, instrumental finish, and quality control. *Critical Reviews in Analytical Chemistry, 43*(4), 224–272. https://doi.org/10.1080/10408347.2012.751787
45. Sahbeni, G., Székely, B. (2022). Spatial modeling of soil salinity using kriging interpolation techniques: a study case in the Great Hungarian Plain. *Eurasian Journal of Soil Science, 11*(2), 102–112. https://doi.org/10.18393/ejss.1013432
46. Seyedmohammadi, J., Esmaeelnejad, L., Shabanpour, M. (2016). Spatial variation modelling of groundwater electrical conductivity using geostatistics and GIS. *Modeling Earth Systems and Environment, 2*(4), 1–10. https://doi.org/10.1007/s40808-016-0226-3
47. Shi, H. J., Wang, X. J., Zhao, Y. J., Xu, M. G., Li, D. W., Guo, Y. (2017). Relationship between soil inorganic carbon and organic carbon in the wheat-maize cropland of the North China Plain. *Plant and Soil, 418*(1), 423–436. https://doi.org/10.1007/s11104-017-3310-1
48. Siqueira, G. M., Dafonte, J. D., Bueno Lema, J., Valcárcel Armesto, M., Silva, Ê. F. F. E. (2014). Using soil apparent electrical conductivity to optimize sampling of soil penetration resistance and to improve the estimations of spatial patterns of soil compaction. *The Scientific World Journal*, *2014*(1), 269480. https://doi.org/10.1155/2014/269480
49. Suello, R. H., Hernandez, S. L., Bouillon, S., Belliard, J. P., Dominguez-Granda, L., Van De Broek, M., Rosado Moncayo, A. M., Veliz, J. R., Ramirez, K. P., Govers, G., Temmerman, S. (2022). Mangrove sediment organic carbon storage and sources in relation to forest age and position along a deltaic salinity gradient. *Biogeosciences, 19*(5), 1571–1585. https://doi.org/10.5194/bg-19-1571-2022
50. Swafo, S. M., Dlamini, P. E. (2023). Utilisation of intrinsic and extrinsic soil information to derive soil nutrient management zones for banana production in a smallholder farm. *Land, 12*(9), 1651. https://doi.org/10.3390/LAND12091651
51. Trangmar, B. B., Yost, R. S., Uehara, G. (1986). Application of geostatistics to spatial studies of soil properties. *Advances in Agronomy*, *38*(C), 45–94. https://doi.org/10.1016/S0065-2113(08)60673-2
52. Tripathi, R., Nayak, A. K., Shahid, M., Raja, R., Panda, B. B., Mohanty, S., Kumar, A., Lal, B., Gautam, P., Sahoo, R. N. (2015). Characterizing spatial variability of soil properties in salt affected coastal India using geostatistics and kriging. *Arabian Journal of Geosciences, 8*(12), 10693–10703. https://doi.org/10.1007/s12517-015-2003-4
53. Walinga, I., Novozamsky, I., Houba, V. J. G., Kithome, M., van der Lee, J. J. (1992). Spectrophotometric determination of organic carbon in soil. *Communications in Soil Science and Plant*

Analysis, 23(15–16), 1935–1944. https://doi.org/10.1080/00103629209368715

54. Walkley, A., Black, I. A. (1934). An examination of the Degtjareff method for determining soil organic matter, and a proposed modification of the chromic acid titration method. *Soil Science, 37*(1), 29–38. https://journals.lww.com/soilsci/citation/1934/01000/AN_EXAMINATION_OF_THE_DEGTJAREFF_METHOD_FOR.3.aspx
55. Wang, F., Guo, R., Zhang, N., Yang, S., Cao, W. (2023). Soil organic carbon storages and bacterial communities along a restored mangrove soil chronosequence in the Jiulong River Estuary: from tidal flats to mangrove afforestation. *Fundamental Research, 3*(6), 880–889. https://doi.org/10.1016/j.fmre.2022.08.019
56. Wang, F., Zhang, N., Yang, S., Li, Y., Yang, L., Cao, W. (2024). Source and stability of soil organic carbon jointly regulate soil carbon pool, but source alteration is more effective in mangrove ecosystem following Spartina alterniflora invasion. *Catena, 235*, 107681. https://doi.org/10.1016/j.catena.2023.107681
57. Webster, R., Oliver, M. A. (2007). Geostatistics for environmental scientists. *Geostatistics for Environmental Scientists: Second Edition*, 1–315. https://doi.org/10.1002/9780470517277
58. Wu, T., Guo, J., Li, G., Jin, Y., Zhao, W., Lin, G., Luo, F. L., Zhu, Y., Jia, Y., Wen, L. (2025). Soil organic carbon contents and their major influencing factors in mangrove tidal flats: a comparison between estuarine and non-estuarine areas. *Ecological Processes, 14*(1). https://doi.org/10.1186/s13717-025-00581-5
59. Xia, S., Song, Z., Van Zwieten, L., Guo, L., Yu, C., Wang, W., Li, Q., Hartley, I. P., Yang, Y., Liu, H., Wang, Y., Ran, X., Liu, C. Q., Wang, H. (2022). Storage, patterns and influencing factors for soil organic carbon in coastal wetlands of China. *Global Change Biology, 28*(20), 6065–6085. https://doi.org/10.1111/gcb.16325
60. Xia, S., Wang, W., Song, Z., Kuzyakov, Y., Guo, L., Van Zwieten, L., Li, Q., Hartley, I. P., Yang, Y., Wang, Y., Andrew Quine, T., Liu, C., Wang, H. (2021). Spartina alterniflora invasion controls organic carbon stocks in coastal marsh and mangrove soils across tropics and subtropics. *Global Change Biology, 27*(8), 1627–1644. https://doi.org/10.1111/gcb.15516
61. Xu, Z., Li, X., Tian, P., Huang, Y., Zhu, Q., Zou, H., Huang, Y., Zhang, Z., Zhang, S., Chen, M., Chen, Y. (2024). Global warming potentials of CO_2 uptake, CH4 emissions, and albedo changes in a restored mangrove ecosystem. *Journal of Geophysical Research: Biogeosciences, 129*(6), e2023JG007924. https://doi.org/10.1029/2023JG007924
62. Yan, R., Feng, J., Fu, T., Chen, Q., Wang, Z., Kang, F., Fang, J., Huang, G., Yang, Q. (2024). Spatial variation of organic carbon storage and aggregate sizes in the sediment of the Zhangjiang mangrove ecosystem. *Catena, 234*, 107545. https://doi.org/10.1016/j.catena.2023.107545
63. Yin, S., Wang, J., Yu, T., Wang, M., Wu, Y., Zeng, H. (2023). Constraints on the spatial variations of soil carbon fractions in a mangrove forest in Southeast China. *Catena, 222*, 106889. https://doi.org/10.1016/j.catena.2022.106889
64. Zarco-Perelló, S., Simões, N. (2017). Ordinary kriging vs inverse distance weighting: spatial interpolation of the sessile community of Madagascar reef, Gulf of Mexico. *PeerJ, 5*, e4078. https://doi.org/10.7717/peerj.4078
65. Zheng, L., Su, M., Zhang, X., Wang, L., Hong, H., Zhang, Q., Zhong, L., Lu, H. (2025). Salinity and inundation drivers shift microbial necromass carbon distribution patterns in estuarine mangrove wetlands. *Geoderma, 460*, 117413. https://doi.org/10.1016/j.geoderma.2025.117413
66. Zhu, Z., Zhang, R., Liu, T., Zheng, H. (2011). Solute accumulation and osmotic adjustment characteristics of the mangrove Avicennia marina under NaCl-induced salinity stress. *Botanica Marina, 54*(3), 335. https://doi.org/10.1515/bot.2011.035